ADVANCED FUNCTIONAL MATERIALS
www.afm-journal.de

A Water Solution Processed Hybrid Electron Transport Layer Simultaneously Enhances Efficiency and Stability in Inverted Structure Organic Solar Cells

Zhaochen Suo, Longyu Li, Jian Liu, Zhaoyang Yao, Chenxi Li, Xiangjian Wan, and Yongsheng Chen**

Achieving both high efficiency and stability in organic solar cells (OSCs) remains a significant challenge. Inverted structure OSCs, compared to those with a normal structure, show great potential for combining high efficiency with enhanced stability. However, despite their improved stability, the efficiencies of inverted OSCs still lag behind those of conventional structure OSCs, largely due to the performance of electron transport layers (ETLs). Herein, a water-soluble hybrid ETL is developed by modifying SnO_2 nanoparticles with an aqueous potassium carboxylate salt, PMA. This modification effectively passivates the oxygen vacancy defects in the SnO_2 nanoparticles and eliminates the light soaking issue observed in the control device. As a result, the PM6:Y6-based device shows an improvement in efficiency from 16.68% to 17.85% with PMA modification. Notably, an exceptional efficiency of 19.07% is achieved for the PM6:BTP-eC9-based device using this hybrid ETL, marking the highest efficiency reported to date for single-junction inverted OSCs. In addition, all tested OSCs with the hybrid ETL demonstrate superior stability under both thermal and light illumination at the maximum power point compared to the control devices. Furthermore, utilizing this water-processed hybrid ETL, a large-area module based on PM6:BO-4Cl is fabricated and shows an outstanding efficiency of 15.02%.

1. Introduction

Organic solar cells (OSCs) have the inherent advantages such as light weight, low-cost, compatibility with large-area printing, and environmental friendliness.[1] Owing to the significant development in active layer molecular innovation and device optimization, power conversion efficiencies (PCEs) of OSCs have surpassed 19%.[2] However, most of OSCs reported in recent years based on non-fullerene acceptor are fabricated using the conventional structure. Despite high efficiencies for conventional structure OSCs, they often suffer from the poor stability primarily due to the corrosive and hygroscopic PEDOT:PSS as the hole transport layer (HTL).[3] In contrast, inverted structure OSCs generally exhibit good stability and have been considered more suitable for large scale manufacture than those with conventional structures.[4] Despite the great application potential of inverted OSC devices, their performances still lag behind current conventional devices in terms of PCEs. It is worth noting that electron transport layers (ETL) play a crucial role on both efficiency and stability for inverted structure OSCs.[5]

In the past decade, several types of ETL materials including polymers materials, small molecules and metal oxide have been explored to enhance the performance of inverted OSCs. Among them, polymer ETLs such as (poly[(9,9-bis(3′-(N,N-dimethylamino)propyl)−2,7-fluorene)-*alt*-2,7-(9,9-dioctylfluorene)] (PFN) and poly[(9,9-bis(3′-(N,N-dimethyl)-N-ethylammonium)-propyl)−2,7-fluorene)-*alt*-2,7-(9,9-dioctylfluorene)]dibromide (PFN-Br) have demonstrated promising device performance.[6] However, they often suffer from the batch-to-batch issue. Small molecules based ETLs, for example, (N,N-dimethylamino)propyl naphthalenediimide (NDI-N) have a definite molecular structure.[7] But unfortunately, the inverted OSCs based on those small molecule ETLs showed much lower efficiencies compared to their corresponding conventional devices. Metal oxides, particularly tin oxide (SnO_2) nanoparticles, have emerged as appealing candidates for ETL in inverted OSCs to hit an excellent performance, owing to

Z. Suo, L. Li, J. Liu, Z. Yao, C. Li, X. Wan, Y. Chen
State Key Laboratory of Elemento-Organic Chemistry
Frontiers Science Center for New Organic Matter
Nankai University
Tianjin 300071, China
E-mail: xjwan@nankai.edu.cn; yschen99@nankai.edu.cn
Z. Suo, L. Li, J. Liu, Z. Yao, C. Li, X. Wan, Y. Chen
The Centre of Nanoscale Science and Technology and Key Laboratory of Functional Polymer Materials
Institute of Polymer Chemistry
College of Chemistry
Nankai University
Tianjin 300071, China
Z. Suo, L. Li, J. Liu, Z. Yao, C. Li, X. Wan, Y. Chen
Renewable Energy Conversion and Storage Center (RECAST)
Nankai University
Tianjin 300071, China

The ORCID identification number(s) for the author(s) of this article can be found under https://doi.org/10.1002/adfm.202409699

DOI: 10.1002/adfm.202409699

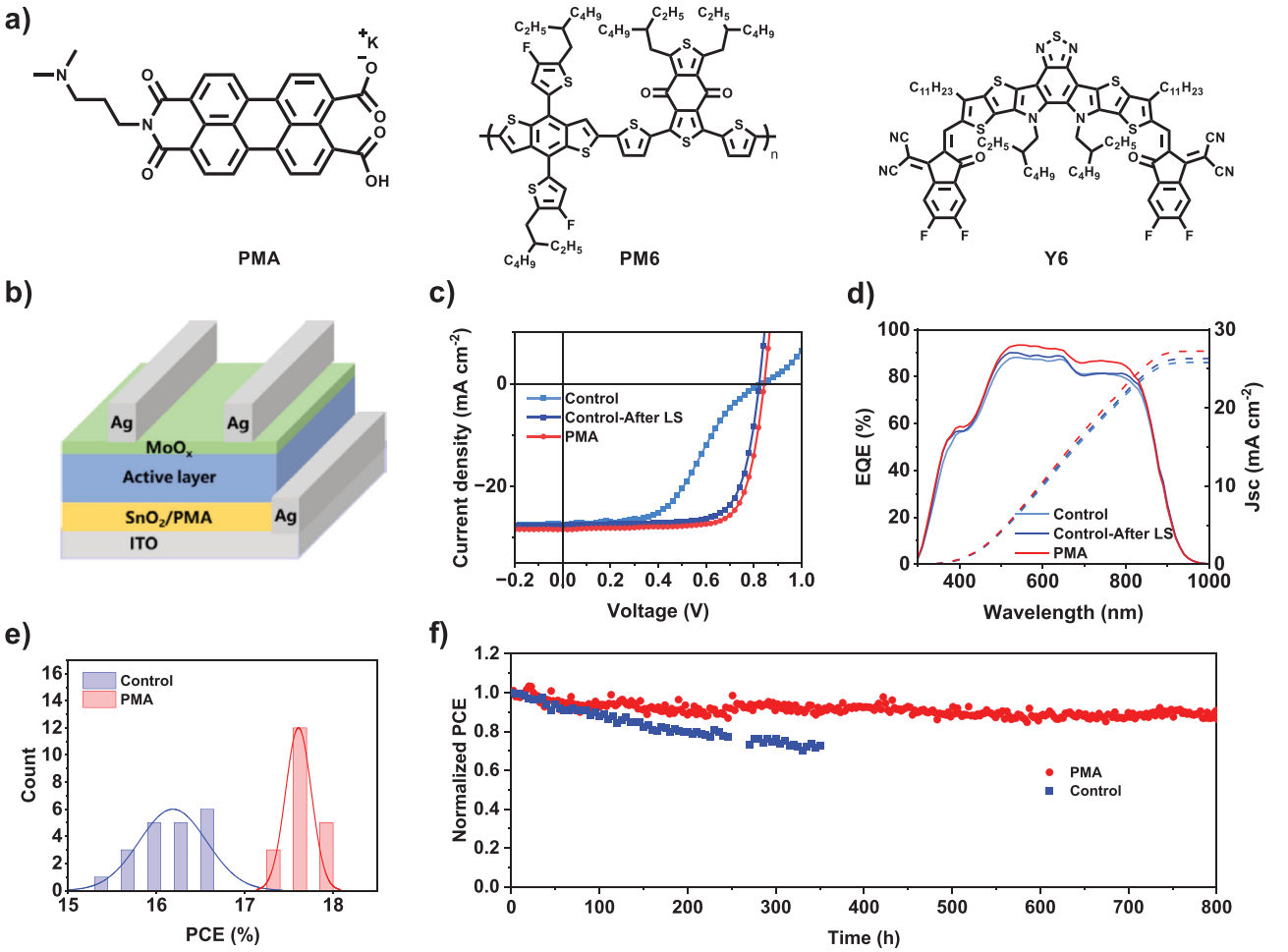

Figure 1. a) Chemical structures of PMA, PM6, and Y6. b) Inverted-device architecture in this work. c) Current density–voltage (*J*–*V*) curves and d) external quantum efficiency (EQE) curves of PM6:Y6 devices based on SnO_2 before and after light soaking 5 min, and PMA modification. e) The histogram of PCEs fitted with Gaussian distributions (solid lines). f) Photostability plots under MPP tracking of control and PMA-based optimal devices based on PM6:Y6 system.

their high visible-light transmittance, excellent charge mobility, lower photocatalytic activity, and chemical stability compared to TiO_2 and ZnO_2.[8] However, various vacancy defects existing on the surface of SnO_2 nanoparticles could generate a mass of recombination centers, hampering the electron transportation and collection within devices.[9] Consequently, when SnO_2 is used as ETL in OSC devices, a serious light soaking (LS) effect is observed, where the OSCs require light exposure, generally several minutes to half an hour or longer time, to achieve stable and optimal performance. However, the devises after LS still show unfavorable performance.[10]

To address the light-soaking effect, various strategies, particularly surface modification, have been developed and achieved promising results. Recently, we employed an interface material called NMA (2-(3-(dimethylamino)propyl)−1,3-dioxo-2,3-dihydro-1H-benzo[de]isoquinoline-6,7-dicarboxylic acid) to modify SnO_2 nanoparticles, effectively eliminating the light-soaking issue observed in devices with SnO_2.[11] Considering that the large fused aromatic backbone is beneficial for electron transport and expected to enhance device performance, we designed and synthesized a new modified molecule named PMA (potassium 9-carboxy-2-(3-(dimethylamino)propyl)−1,3-dioxo-2,3-dihydro-1H-benzo[10,5]anthra[2,1,9-def]isoquinoline-8-carboxylate) to modify the SnO_2 interface (**Figure 1a**). First, the carboxylate anion efficiently coordinates with Sn atoms, thereby passivating the oxygen vacancies of SnO_2 to inhibit surface defects and charge recombination. Second, as a potassium carboxylate salt, PMA exhibits excellent water-solubility, which is benefit to form a totally water-processed hybrid ETL, and ultimately, making it more environmentally friendly for large-scale solar cell manufacturing. Moreover, the large fused aromatic main backbone paves the way for electron transport, thereby boosts the electron transport capacity.

Consequently, when PMA was introducing as a modifying material on the SnO_2 ETL, various different typical systems exhibited simultaneous improvements in both performance and stability. The PM6:Y6 based inverted OSCs shows a significant increase in PCE from 16.68% to 17.85% with PMA modification. For the PM6:BTP-eC9 based device, an outstanding performance of 19.07% was achieved, enabled by the hybrid ETL. To our

Table 1. Device characteristics of the OSCs based on different ETLs.

ITO/ETL/PM6:Y6/MoOx/Ag	V_{OC} [V]	J_{SC} [mA cm^{-2}]	$J_{cal.}$ [b] [mA cm^{-2}]	FF [%]	PCE[a] [%]
Control	0.831	27.41	25.83	46.01	10.48
Control-After LS	0.823	27.54	26.32	73.54	16.68 (16.19 ± 0.37)
PMA	0.844	28.40	27.26	74.82	17.85 (17.61 ± 0.14)

[a] The average photovoltaic parameter was calculated from 20 independent devices; [b] Current densities calculated from EQE curves.

knowledge, this is the highest PCE for inverted single-junction OSCs. Notably, all OSCs measured with the hybrid ETL demonstrated significantly better stability under both thermal and continuous 100 mW cm^{-2} light illumination at the maximum power point (MPP) compared to the control devices. In addition, a module with area 13.5 cm^2 based on PM6:BO-4Cl was fabricated using this hybrid ETL, achieving an outstanding PCE of 15.02%.

2. Results and Discussion

2.1. Device Performance and Stability

PMA was synthesized following the reported method,[12] and the detailed synthesis procedure and characterization are provided in the supporting information. For the preparation of the hybrid ETL, a film of SnO_2 was initially prepared by casting from an aqueous solution of SnO_2 nanoparticles. To enhance the film quality, a polymer PAA was added to the SnO_2 nanoparticle solution following the literature method.[13] After thermal annealing, a layer of PMA was cast onto the surface of the SnO_2 film to form the hybrid ETL. It should be noted that the thin film of SnO_2 is water-resistant after thermal annealing treatment, ensuring that the second layer of PMA can be cast from its water solution.

To evaluate photovoltaic performance of this hybrid ETL, PM6:Y6, one of the classic OSC systems (see chemical structure in Figure 1b) was selected to fabricate devices with an inverted structure as ITO/ETL/PM6:Y6/MoOx/Ag (Figure 1a). For the control device, there existed a severe light soaking phenomenon, as shown in Figure S4 (Supporting Information), the freshly prepared device showed a distinct S-shaped *J*-*V* curve (Figure 1c) and yielded a low PCE of 10.48%. The device's performance gradually improved to a PCE of 16.68% after 5 min continuous illumination under a solar simulator. In contrast, the light soaking was eliminated after PMA modification and a remarkably improved PCE of 17.85% was achieved (**Table 1**). The EQE curves of the devices with and without PMA are illustrated in Figure 1d. The integrated J_{SC} values obtained from the EQE curves were 25.83 and 26.32 mA cm^{-2} for the control device before and after light-soaking, and 27.26 mA cm^{-2} for the PMA modified device, respectively, which aligned well with the values obtained from the *J*–*V* curves. The device modified by PMA exhibited an enhanced photo response nearly in the whole absorption range than the control cell. As the control devices require enough illumination to achieve its optimal performance, all subsequent reports of them in this article are based on the performance after light soaking. The histograms and corresponding Gaussian distribution of PCE counting for 20 individual control and PMA-based devices are shown in Figure 1e and the impressive efficiency improvement could be observed.

The stability is one of the key factors restricting the practical application of OSCs.[14] To explore the influence of the PMA hybrid layer on the device stability, we measured the thermal and light stability for the devices with and without PMA modification. As shown in Figure S5 (Supporting Information), the PM6:Y6 device based on SnO_2/PMA maintained 90.6% of its initial PCE after annealing at 85 °C in N_2 atmosphere for 200 h, whereas the PCE of the control device significantly reduced to 80.6%. We further tested the operational stability operated at the maximum power point (MPP) under continuous 100 mW cm^{-2} light illumination. As shown in Figure 1f, the PCE of the control device substantially decreased to 72.8% of its initial value after 350 h. Notably, the device with PMA still remained at 90.7% after 800 h, exhibited a fitting T_{80} of 6515 h (Figure S5). Compared to previous reports based on SnO_2 ETL, this result is the first report with T_{80} exceeding 1000 h,[9c,15] ranking PMA based devices as the photostability champion of OSCs with SnO_2 ETLs.

2.2. Characterization of SnO_2/PMA

To investigate the mechanism for the distinguish improvement of the device with surface PMA modification, firstly, we conducted a theory analysis for the interaction of PMA and SnO_2. As shown in **Figure 2a**, five different possible coordination sites, including α-O, β-O, γ-O, α-N, and β-N, have the potentials to form interface coordination with the SnO_2 surface. However, considering the steric effects, it is difficult for β-N to coordinate effectively with SnO_2 (Figure S6, Supporting Information). To explore the most thermodynamically stable configuration between PMA and SnO_2, DFT, as implemented in Vienna ab initio simulation package (VASP), was used to figure out the calculations presented here (Figure 2b). Compared with other positions, α-O can form the most stable coordination structure with Sn atom on the surface of SnO_2, leaving a significant large adsorption energy of −241.89 kJ mol^{-1} and shortest coordination distance of 2.17 Å. This might be according to the higher electronegativity of the α-O atom of the carboxylate anion. The stable coordination conformation between SnO_2 and PMA is expected to effectively passivate the surface oxygen vacancies of SnO_2 and furthermore improve the efficiency and stability of OSC devices.

X-ray photoelectron spectra (XPS) measurement was carried out to signifying the interaction between PMA and SnO_2 (Figure 2c). N 1s at 400.1 eV were detected to confirm the adherence of PMA on the SnO_2. The Sn 3d $_{3/2}$ and Sn 3d $_{5/2}$ peaks of the SnO_2/PMA film located at 495.2 and 486.8 eV, which were shifted

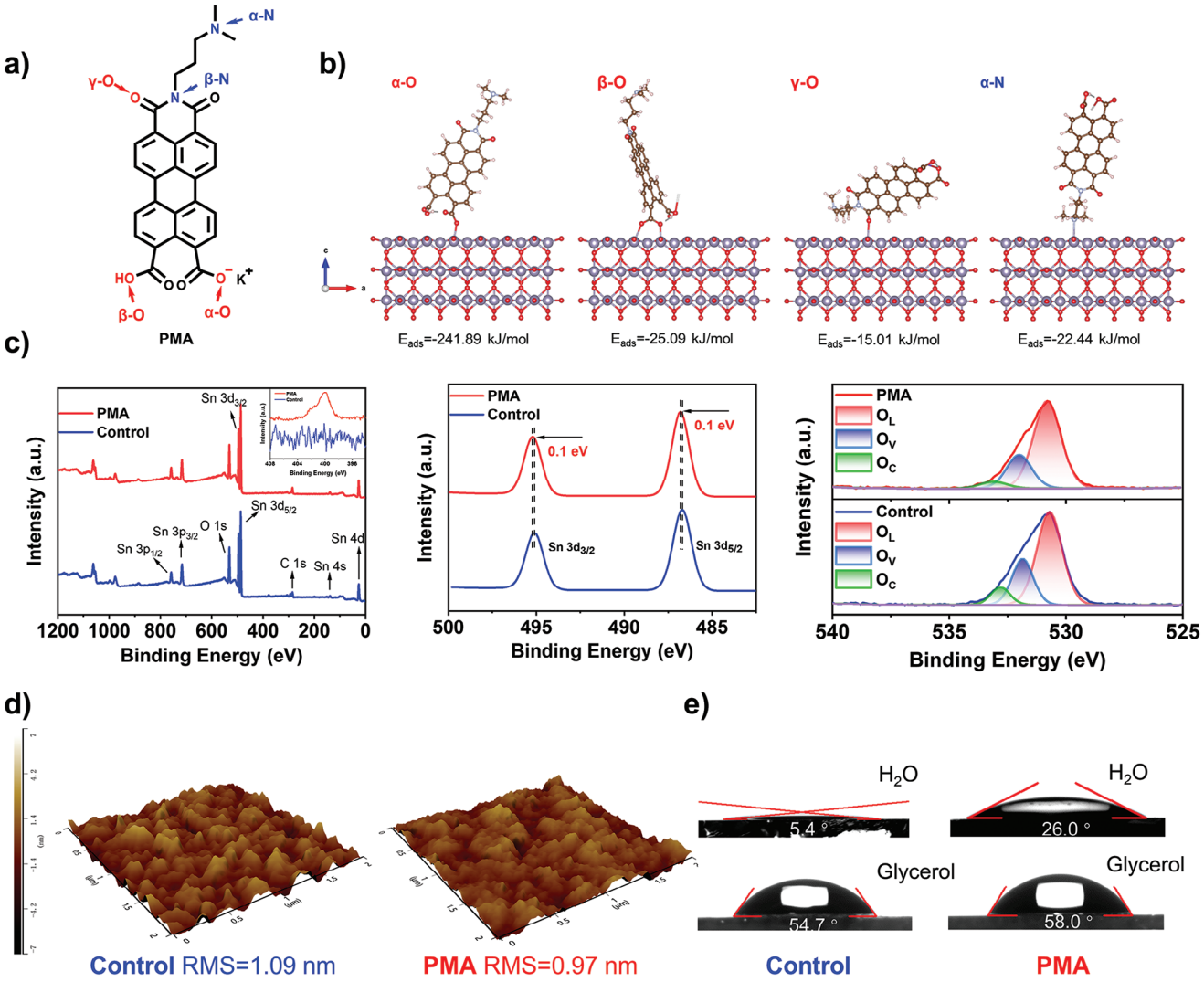

Figure 2. a) Molecular structure of PMA marked with five possible coordination sites. b) Optimized configurations of PMA absorbed on SnO_2 via different sites, including α-O, β-O, γ-O, and α-N. c) X-ray photoelectron spectroscopy (XPS) plots of control and PMA based ETL films. N 1s core level spectrum, Sn 3d core level spectrum and O 1s core level spectrum, respectively. d) Atomic force microscopy (AFM) height images of the corresponding films. e) Contact angles of the corresponding films.

to the higher binding energy direction by 0.1 eV, indicating that the Sn atoms of SnO_2 surface can interact well with PMA.[16] The O 1 s spectra of the PMA-modified and control SnO_2 films are shown in Figure 2c, which could be divided into lattice oxygen (O_L), oxygen vacancies (O_V), and chemisorbed oxygen (O_C). The percentage of oxygen vacancies in the PMA-modified SnO_2 film was 24.7%, which is lower than the 26.5% observed in the control one.[17] This correlates well with the calculation results. The reduction in oxygen vacancies is beneficial for attenuating the carrier recombination and eventually improving the functionality of the device. Moreover, the passivation of oxygen vacancies by Sn-carbonate group coordination could also alleviate the initial burn-in loss under illumination, therefore improve the device stability.[15]

Moreover, atomic force microscopy (AFM) was used to investigate the surface roughness of the films (Figure 2d). Compared with the control film whose root-mean-square roughness (RMS) is 1.09 nm, PMA modified one has a slightly smoother surface with an RMS of 0.97 nm. The contact angles have been measured before and after PMA modification in Figure 2e. First, the water dispersed SnO_2 layer has a significant small water contact angle, which makes it easy for PMA aqueous to spin on it and form a totally water-processed hybrid ETL. In addition, the surface energy (γ_s) can also be fine-tuned after PMA modification. Calculated by the Wu model,[18] the modified film's surface energy is 81.4 mJ m^{-2}, slightly lower than the control film (Table S1, Supporting Information). The aforementioned results would potentially benefit to higher device performance.

2.3. Exciton Dynamics

The charge generation, transport, and recombination behaviors are essential to evaluate the quality of ETLs. First, to investigate

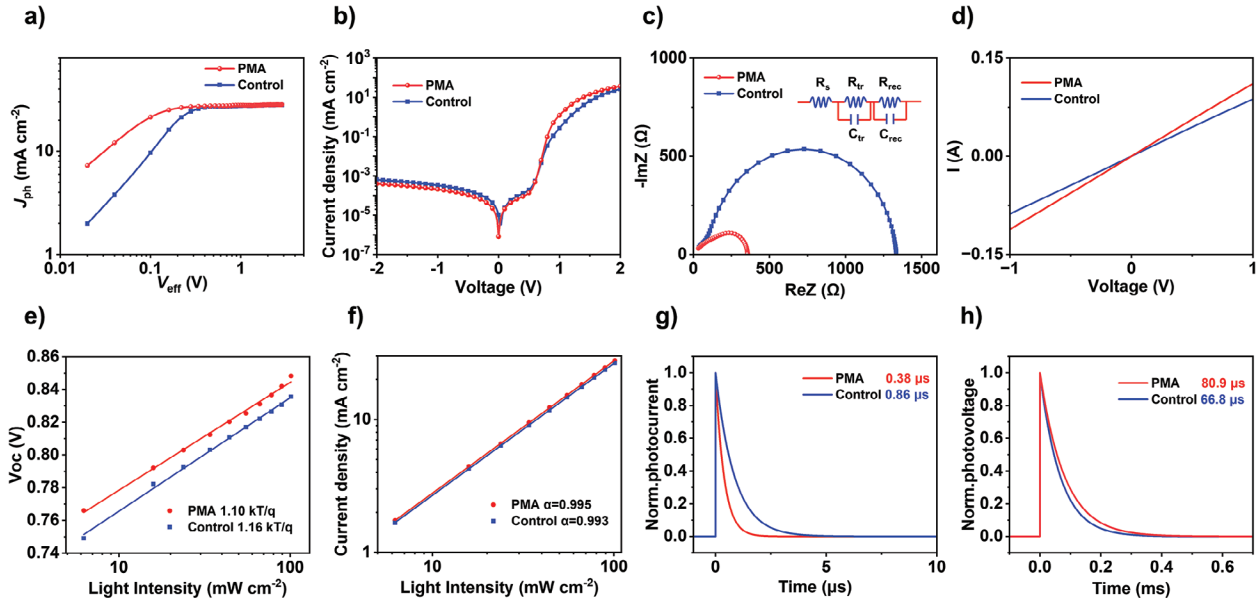

Figure 3. a) Photocurrent density versus effective voltage (J_{ph}–V_{eff}) characteristics for the devices based on different ETLs. b) *J*–*V* characteristics in dark of devices with different ETLs. c) Nyquist plots of devices based on SnO_2 and SnO_2/PMA. d) The conductivity curves of different ETLs. e) V_{OC} values of the photovoltaic devices versus light intensity. f) J_{SC} values of the photovoltaic devices versus light intensity. g) Transient photocurrent and h) transient photovoltage measurements of devices based on SnO_2 and SnO_2/PMA analyzed by a one order exponential decline model.

the effects of surface modification on exciton dissociation properties, the dependence of photocurrent density (J_{ph}) on effective voltage (V_{eff}) for the two devices was evaluated (**Figure 3a**).[19] The calculation details of P_{diss} are given in the Supporting Information. PMA-based OSC afforded excellent exciton dissociation efficiencies (P_{diss}) of 98.5% at short-circuit current and 88.8% at maximal power point condition. In contrast, the control one only exhibited lower P_{diss} of 97.8% and 84.0% at these two conditions, respectively. The higher P_{diss} values demonstrate a better charge extraction capacity of the PMA-modified OSC, which resulted in concurrent enhancement of J_{SC} and FF.

Second, the electron transport capability was characterized in control and target devices. Figure 3b illustrates the dark *J*–*V* characteristics of the OSCs. Under a reverse bias voltage, a reduced leakage current of the PMA-based device indicates the suppression of hole injection at the cathode interface; At a positive bias, an enhanced rectification ratio is attributed to a smaller series resistance and improved carrier injection process.[20] Figure 3c provides the Nyquist plots probed at V_{OC} under dark conditions for the electrical impedance spectroscopy (EIS).[21] The double RC circuit model was used to fit the EIS spectra to obtain the series resistance (R_s), charge transport resistance (R_{tr}), and charge recombination resistance (R_{rec}). Because the SnO_2 films were produced by using commercially available colloidal dispersions of SnO_2 nanoparticles, which consistently contained defects stemming from crystal imperfections in the SnO_2 nanoparticles and the presence of residual organic ligands and additives used to stabilize the colloidal dispersion. These defects compromise the interface with the active layer in the control devices, thus increasing the charge transport resistance of them. However, according to the XPS results discussed before, with PMA modified, the defects on the SnO_2 surface were passivated to a certain extent. Therefore, the R_s and R_{tr} of the target device were 29.2 and 181 Ω, respectively, which are lower than those for the control device (30.5 Ω and 1.17 kΩ, respectively), and a higher R_{rec} of the target device (102 Ω) than that of control one (84.3 Ω). This indicates an enhanced charge transport and suppressed interfacial charge recombination, and in turn a less interface potential loss between inorganic SnO_2 and the organic photoactive layer.[22] Moreover, the conductivity of the ETLs were estimated under a bias voltage of 1 V (Figure 3d).[23] The PMA modified ETL exhibits a conductivity of 5.28×10^{-4} S m^{-1}, higher than that of the control one with a value of 4.15×10^{-4} S m^{-1}. The higher conductivity might attribute to the large fused aromatic main backbone derived from perylene diimide, which is beneficial for electron transport/hoping.[24]

To further verify the carrier recombination in the control and PMA-based device, The light intensity-dependent V_{OC} data following the equation $V_{OC} \propto nkT/q \ln(I)$ show that target device exhibits a smaller slope (1.10 kT/q) near to 1 kT/q (Figure 3e), where k is the Boltzmann constant, T is temperature, and q is the elementary charge. The smaller slope of the SnO_2/PMA-based device demonstrates that PMA modification can effectively suppress trap-assisted recombination, which benefits the enhancement of J_{SC} and FF. The relationship between the J_{SC} and light intensity (P_{light}) enables a semi-quantitative evaluation of the charge recombination behavior in an OSC. After modification, the exponent α of the target device ($J_{SC} \propto I^{\alpha}$) increased from 0.993 to 0.995 (Figure 3f), indicating weaker bimolecular recombination, leading to improved J_{SC} and FF.[25] Furthermore, transient photocurrent (TPC) and transient photovoltage (TPV) measurements were carried out to investigate the charge extraction and recombination properties (Figure 3g,h). Compared with the control device, the PMA-modified device exhibited a much shorter charge extraction time (0.38 μs vs 0.86 μs) and a longer carrier lifetime (80.8 μs vs 66.8 μs). These results suggest

Table 2. Summary of device parameters for optimized OSCs.

ITO/ETL/AL/MoO_x/Ag		V_{oc} [V]	J_{sc} [mA cm^{-2}]	$J_{cal.}$[b] [mA cm^{-2}]	FF [%]	PCE[a] [%]
PM6:L8-BO	Control	0.863	26.67	25.66	75.56	17.33 (17.18 ± 0.15)
	PMA	0.886	27.10	26.26	77.23	18.59 (18.35 ± 0.12)
PM6:CH23	Control	0.863	26.92	25.61	75.00	17.43 (17.17 ± 0.19)
	PMA	0.880	27.03	26.00	77.80	18.51 (18.36 ± 0.12)
PM6:BTP-eC9	Control	0.826	27.18	26.54	75.62	16.98 (16.80 ± 0.16)
	PMA	0.851	28.38	27.44	78.95	19.07 (18.91 ± 0.09)
PM6:BO4Cl	Control	0.826	27.59	26.39	74.55	16.98 (16.76 ± 0.28)
	PMA	0.835	28.73	27.33	77.68	18.63 (18.27 ± 0.27)
	PMA[c]	4.95	4.15		73.23	15.02

[a] The average photovoltaic parameters calculated from eight independent devices; [b] Current densities calculated from EQE curves; [c] Module area = 13.5 cm^2.

that PMA modification effectively could improve charge extraction efficiency and decrease recombination behavior. All of the above analyses consistent well with the improved photovoltaic performance observed in the device with PMA modification.

2.4. Generality

To assess the generality of this hybrid ETL, we fabricated inverted devices using four typical active layer systems, namely, PM6:BO-4Cl, PM6:L8-BO, PM6:CH23, and PM6:BTP-eC9. It should be noted that only a few cases with efficiencies over 18% have been reported for inverted OSCs to date.[9a,21b,23,24,26] Impressively, with this hybrid ETL, PCEs of all four inverted OSCs have been boosted significantly with values over 18.5% due to simultaneously enhanced V_{oc}, J_{SC}, and FF (**Table 2**, **Figures** 4a, and S7, Supporting Information). Moreover, the thermal and light stability of all four devices significantly improved after modification with PMA (Figure S8, Supporting Information). Notably, the device based on the PM6:BTP-eC9 system demonstrated a high PCE

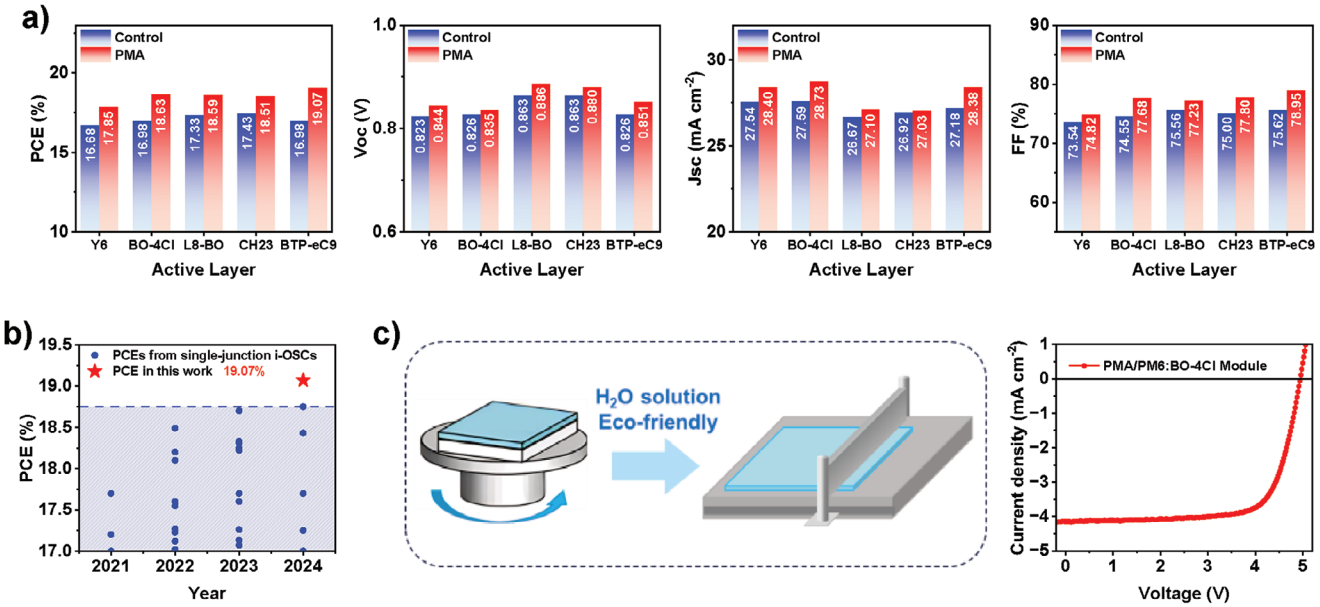

Figure 4. a) PCE, V_{OC}, J_{SC}, and FF of PM6:NFA devices with or without PMA. b) PCE comparison of our results with representative inverted OSCs reported in the literature. c) Application of PMA in large-area fabrication. The photovoltaic results of the large area module with blade-coated PMA as hybrid ETL and PM6:BO-4Cl as active layer.

of 19.07%, marking the highest efficiency for inverted single-junction OSCs. In addition, the PM6:BTP-eC9 device with the hybrid ETL maintained 87.7% of its initial PCE after nearly 500 h of continuous 1 sun illumination under MPP tracking. In contrast, the control device had already degraded by 20% of its initial PCE after just 100 h of illumination.

Water-soluble PMA and the aqueous colloidal dispersed commercial SnO_2 nanoparticles make the hybrid ETL more environmentally friendly for large-scale solar cell manufacturing. Moreover, the boosting efficiencies of PMA-based OSCs also provided more opportunities for high-efficiency large-area modules. Thus, a blade-coating processed module based on this hybrid ETL with PM6:BO-4Cl as active layer was fabricated and demonstrated a high PCE of 15.02% (Figure 4c).

3. Conclusion

In summary, we have designed a molecule named PMA to form a water solution processed hybrid ETL with SnO_2 for inverted OSCs. The surface modification effectively reduces the oxygen defects of the SnO_2 surface and enhances the electron transport and collection capabilities, therefore significantly improving the efficiency and stability for all tested typical photovoltaic devices. For instance, for the typical PM6:Y6 system, the PMA-based OSCs achieved a PCE of 17.85%, surpassing the control device with a PCE of 16.68%. Furthermore, 90.7% of the initial PCE was maintained after 800 h under MPP tracking test (T_{80} = 6515 h), whereas the control one only remained 72.8% after 350 h. Moreover, the hybrid ETL also demonstrated good generality in simultaneously improvement of efficiencies and stabilities for other four typical active layer systems based devices. Notably, the PM6:BTP-eC9 based device with PMA modification achieved a remarkable PCE of 19.07%, which is the highest efficiency reported to date for single-junction inverted structure OSCs. Meanwhile, under MPP tracking, the PM6: BTP-eC9 device with the hybrid ETL maintained 87.7% of its initial PCE after nearly 500 h of continuous illumination. In contrast, after only 100 h, the control device has degraded by 20% of its initial PCE. Moreover, with this hybrid ETL, a PCE of 15.02% was achieved for PM6:BO-4Cl based module via blade coating, indicating the potential application in the manufacturing of large-area OSCs. Overall, this research presents a promising ETL approach for achieving high efficiency and stability in OSCs, and also paves the way to an effective ETL technology for future large-scale manufacturing.

Supporting Information

Supporting Information is available from the Wiley Online Library or from the author.

Acknowledgements

The authors gratefully acknowledge the financial support from National Natural Science Foundation of China (52025033, 52373189, 21935007, and 22361132530) and Ministry of Science and Technology of the People's Republic of China (2022YFB4200400, 2019YFA0705900, 2023YFE0210400, and 2022YFA1203304).

Conflict of Interest

The authors declare no conflict of interest.

Data Availability Statement

The data that support the findings of this study are available in the supplementary material of this article.

Keywords

electron transport layers, organic solar cells, SnO_2, stability

Received: June 4, 2024
Revised: July 26, 2024
Published online:

[1] a) X. J. Wan, C. X. Li, M. T. Zhang, Y. S. Chen, *Chem. Soc. Rev.* **2020**, *49*, 2828; b) Y. H. Liu, B. W. Li, C. Q. Ma, F. Huang, G. T. Feng, H. Z. Chen, J. H. Hou, L. P. Yan, Q. Y. Wei, Q. Luo, Q. Y. Bao, W. Ma, W. Liu, W. W. Li, X. J. Wan, X. T. Hu, Y. C. Han, Y. W. Li, Y. H. Zhou, Y. P. Zou, Y. W. Chen, Y. F. Li, Y. S. Chen, Z. Tang, Z. C. Hu, Z. G. Zhang, Z. S. Bo, *Sci. China Chem.* **2022**, *65*, 224; c) Y. H. Liu, B. W. Liu, C. Q. Ma, F. Huang, G. T. Feng, H. Z. Chen, J. H. Hou, L. P. Yan, Q. Y. Wei, Q. Luo, Q. Y. Bao, W. Ma, W. Liu, W. W. Li, X. J. Wan, X. T. Hu, Y. C. Han, Y. W. Li, Y. H. Zhou, Y. P. Zou, Y. W. Chen, Y. Q. Liu, L. Meng, Y. F. Li, Y. S. Chen, Z. Tang, Z. C. Hu, Z. G. Zhang, Z. S. Bo, *Sci. China Chem.* **2022**, *65*, 1457; d) G. Zhang, F. R. Lin, F. Qi, T. Heumuller, A. Distler, H. J. Egelhaaf, N. Li, P. C. Y. Chow, C. J. Brabec, A. K. Jen, H. L. Yip, *Chem. Rev.* **2022**, *122*, 14180.

[2] a) L. X. Meng, Y. M. Zhang, X. J. Wan, C. X. Li, X. Zhang, Y. B. Wang, X. Ke, Z. Xiao, L. M. Ding, R. X. Xia, H. L. Yip, Y. Cao, Y. S. Chen, *Science* **2018**, *361*, 1094; b) J. Yuan, Y. Q. Zhang, L. Y. Zhou, G. C. Zhang, H. L. Yip, T. K. Lau, X. H. Lu, C. Zhu, H. J. Peng, P. A. Johnson, M. Leclerc, Y. Cao, J. Ulanski, Y. F. Li, Y. P. Zou, *Joule* **2019**, *3*, 1140; c) C. Li, J. D. Zhou, J. L. Song, J. Q. Xu, H. T. Zhang, X. N. Zhang, J. Guo, L. Zhu, D. H. Wei, G. C. Han, J. Min, Y. Zhang, Z. Q. Xie, Y. P. Yi, H. Yan, F. Gao, F. Liu, Y. M. Sun, *Nat. Energy* **2021**, *6*, 605; d) L. Zhu, M. Zhang, J. Q. Xu, C. Li, J. Yan, G. Q. Zhou, W. K. Zhong, T. Y. Hao, J. L. Song, X. N. Xue, Z. C. Zhou, R. Zeng, H. M. Zhu, C. C. Chen, R. C. I. MacKenzie, Y. C. Zou, J. Nelson, Y. M. Zhang, Y. M. Sun, F. Liu, *Nat. Mater.* **2022**, *21*, 656; e) Z. Yao, X. Wan, C. Li, Y. Chen, *Acc. Mater. Res.* **2023**, *4*, 772; f) S. Guan, Y. Li, C. Xu, N. Yin, C. Xu, C. Wang, M. Wang, Y. Xu, Q. Chen, D. Wang, L. Zuo, H. Chen, *Adv. Mater.* **2024**, *36*, 3422400; g) Y. Sun, L. Wang, C. Guo, J. Xiao, C. Liu, C. Chen, W. Xia, Z. Gan, J. Cheng, J. Zhou, Z. Chen, J. Zhou, D. Liu, T. Wang, W. Li, *J. Am. Chem. Soc.* **2024**, *146*, 12011.

[3] a) M. P. de Jong, L. J. van Ijzendoorn, M. J. A. de Voigt, *Appl. Phys. Lett.* **2000**, *77*, 2255; b) J. Cameron, P. J. Skabara, *Mater. Horiz.* **2020**, *7*, 1759.

[4] a) X. Xu, J. Y. Xiao, G. C. Zhang, L. Wei, X. C. Jiao, H. L. Yip, Y. Cao, *Sci. Bull.* **2020**, *65*, 208; b) Y. Han, H. Dong, W. Pan, B. Liu, X. Chen, R. Huang, Z. Li, F. Li, Q. Luo, J. Zhang, Z. Wei, C. Q. Ma, *ACS Appl. Mater. Interfaces* **2021**, *13*, 17869; c) Y. X. Li, B. Huang, X. N. Zhang, J. W. Ding, Y. Y. Zhang, L. E. Xiao, B. X. Wang, Q. Cheng, G. S. Huang, H. Zhang, Y. G. Yang, X. Y. Qi, Q. Zheng, Y. Zhang, X. H. Qiu, M. H. Liang, H. Q. Zhou, *Nat. Commun.* **2023**, *14*, 1241; d) X. Liu, Z. Zheng, J. Wang, Y. Wang, B. Xu, S. Zhang, J. Hou, *Adv. Mater.* **2022**, *34*, 2106453.

[5] a) H. Tang, Y. Bai, H. Zhao, X. Qin, Z. Hu, C. Zhou, F. Huang, Y. Cao, *Adv. Mater.* **2024**, *36*, 2212236; b) P. Jiang, L. Hu, L. Sun, Z. Li, H. Han, Y. Zhou, *Chem. Sci.* **2022**, *13*, 4714.

[6] F. Huang, H. Wu, D. Wang, W. Yang, Y. Cao, *Chem. Mater.* **2004**, *16*, 708.
[7] Q. Kang, L. Ye, B. Xu, C. An, S. J. Stuard, S. Zhang, H. Yao, H. Ade, J. Hou, *Joule* **2019**, *3*, 227.
[8] a) L. Xiong, Y. Guo, J. Wen, H. Liu, G. Yang, P. Qin, G. Fang, *Adv. Funct. Mater.* **2018**, *28*, 1802757; b) Y. Jiang, L. Sun, F. Jiang, C. Xie, L. Hu, X. Dong, F. Qin, T. Liu, L. Hu, X. Jiang, Y. Zhou, *Mater. Horiz.* **2019**, *6*, 1438.
[9] a) R. Yu, X. Wei, G. Wu, T. Zhang, Y. Gong, B. Zhao, J. Hou, C. Yang, Z. Tan, *Energy Environ. Sci.* **2022**, *15*, 822; b) H. Gao, X. Wei, R. Yu, F.-Y. Cao, Y. Gong, Z. Ma, Y.-J. Cheng, C.-S. Hsu, Z. Tan, *Adv. Opt. Mater.* **2022**, *10*, 2102031; c) J. Wu, F. Tang, S. Wu, Y. Li, L. Xiao, X. Zhu, X. Peng, *Adv. Energy Mater.* **2024**, *14*, 2302932.
[10] a) R. Munir, E. Cieplechowicz, R. M. Lamarche, R. Chernikov, S. Trudel, G. C. Welch, *Adv. Mater. Interfaces* **2021**, *9*, 2101918; b) L. D. Mario, D. G. Romero, H. Wang, E. K. Tekelenburg, S. Meems, T. Zaharia, G. Portale, M. A. Loi, *Adv. Mater.* **2023**, *36*, 2301404.
[11] Z. Suo, Z. Xiao, S. Li, J. Liu, Y. Xin, L. Meng, H. Liang, B. Kan, Z. Yao, C. Li, X. Wan, Y. Chen, *Nano Energy* **2023**, *118*, 109032.
[12] a) K. Huth, T. Heek, K. Achazi, C. Kuhne, L. H. Urner, K. Pagel, J. Dernedde, R. Haag, *Chem.-Eur. J.* **2017**, *23*, 4849; b) S. W. Tam-Chang, W. Seo, I. K. Iverson, *J. Org. Chem.* **2004**, *69*, 2719.
[13] M. Kim, J. Jeong, H. Lu, T. K. Lee, F. T. Eickemeyer, Y. Liu, I. W. Choi, S. J. Choi, Y. Jo, H.-B. Kim, S.-I. Mo, Y.-K. Kim, H. Lee, N. G. An, S. Cho, W. R. Tress, S. M. Zakeeruddin, A. Hagfeldt, J. Y. Kim, M. Gratzel, D. S. Kim, *Science* **2022**, *375*, 302.
[14] Q. Burlingame, M. Ball, Y.-L. Loo, *Nat. Energy* **2020**, *5*, 947.
[15] D. Kim, S. Lee, C.-M. Oh, I.-W. Hwang, C. Yoon, H. Kim, J. Byeon, K. Lee, S. Hong, *Sol. RRL* **2024**, *9*, 2300987.
[16] a) S. Guang, J. Yu, H. Wang, X. Liu, S. Qu, R. Zhu, W. Tang, *J. Energy Chem.* **2021**, *56*, 496; b) J. Y. Jiahao Xi, J. Du, X. Yan, J. Tian, *Small* **2022**, *18*, 2203519.
[17] a) S. Liu, S. Gao, Z. Wang, T. Fei, T. Zhang, *Sens. Actuators, B* **2019**, *290*, 493; b) Q. Zeng, Y. Cui, L. Zhu, Y. Yao, *Mater. Sci. Semicond. Process.* **2020**, *111*, 104962.
[18] J. Comyn, *Int. J. Adhes. Adhes.* **1992**, *12*, 145.
[19] P. W. M. Blom, V. D. Mihailetchi, L. J. A. Koster, D. E. Markov, *Adv. Mater.* **2007**, *19*, 1551.
[20] a) Y. L. Ma, M. Zhang, S. Wan, P. Yin, P. S. Wang, D. D. Cai, F. Liu, Q. D. Zheng, *Joule* **2021**, *5*, 197; b) J. Yao, S. Y. Ding, R. Zhang, Y. Bai, Q. J. Zhou, L. Meng, E. Solano, J. A. Steele, M. B. J. Roeffaers, F. Gao, Z. G. Zhang, Y. F. Li, *Adv. Mater.* **2022**, *34*, 2203690.
[21] a) M. A. Afroz, C. A. Aranda, N. K. Tailor, Yukta, P. Y., M. M. Tavakoli, M. Saliba, S. Satapathi, *ACS Energy Lett.* **2021**, *6*, 3275; b) Y. Yu, Y. Cui, T. Zhang, Z. Chen, Y. Xiao, W. Wang, Y. Yang, N. Yang, J. Hou, *Adv. Funct. Mater.* **2023**, *33*, 2306095.
[22] a) L. Lu, Q. Kang, C. Yang, B. Xu, J. Hou, *J. Phys. Chem. C* **2018**, *122*, 19328; b) N. Tokmoldin, C. Deibel, D. Neher, S. Shoaee, *Adv. Energy Mater.* **2024**, *14*, 2401130.
[23] S. Li, Z. Xiao, J.-J. Li, Z.-Y. Hu, Y. Yang, B. Kan, D.-S. Guo, X. Wan, Z. Yao, C. Li, Y. Chen, *Sci. China Chem.* **2023**, *66*, 195.
[24] S. Li, Q. Fu, L. Meng, X. Wan, L. Ding, G. Lu, G. Lu, Z. Yao, C. Li, Y. Chen, *Angew. Chem., Int. Ed.* **2022**, *61*, e202207397.
[25] J. Ge, L. Xie, R. Peng, B. Fanady, J. Huang, W. Song, T. Yan, W. Zhang, Z. Ge, *Angew. Chem., Int. Ed.* **2020**, *59*, 2808.
[26] a) Z. Suo, J. Liu, S. Li, Z. Yao, C. Li, X. Wan, Y. Chen, *Mater. Chem. Front.* **2024**, *8*, 562; b) M. Cui, Q. Rong, R. Wang, D. Ye, N. Li, L. Nian, *Small* **2024**, *20*, 2311339; c) S. Yang, H. Yu, *Chem. Eng. J.* **2023**, *452*, 139658; d) R. Yu, R. Shi, H. Liu, G. Wu, Z. Ma, H. Gao, Z. He, Z. a. Tan, *Adv. Energy Mater.* **2022**, *12*, 2201306; e) Q. Huang, J. Jing, K. Zhang, Y. Chen, A. Song, Z. Liu, F. Huang, *J. Mater. Chem. A* **2022**, *10*, 23973; f) Y. Xin, H. Liu, X. Dong, Z. Xiao, R. Wang, Y. Gao, Y. Zou, B. Kan, X. Wan, Y. Liu, Y. Chen, *J. Am. Chem. Soc.* **2024**, *146*, 3363.